Int J Syst Assur Eng Manag
https://doi.org/10.1007/s13198-018-0734-9

ORIGINAL ARTICLE

Wind energy conversion system based on dual stator induction generator controlled by nonlinear backstepping and pi controllers

Meryem Benakcha[1] · Leila Benalia[1] · Abdelkrim Ammar[2] · Amor Bourek[2]

Received: 18 May 2017 / Revised: 6 December 2017

Abstract To capture wind energy and to produce electrical power, many conversion systems have been proposed. This work treats also the modeling and the control of dual stator induction generator DSIG integrated in wind energy conversion system. In order to increase the flow of the power to the grid and to ensure an optimum operating point, it is very important to act on the generator side controllers and the conversion system output variables. The Proportional integral PI controllers have been widely used to control alternative machines. In this case, the inverters, which fed the DSIG, are controlled simultaneously with a displaced angle of 30°. So, the synthesis PI gains still difficult. To solve this problem, a nonlinear backstepping control is proposed. For that, the suggested study presents the comparison of the performances of the two strategies. Different simulation tests are conducted to evaluate the efficiency and the validity of the proposed control strategies. We notice that in the steady state, the two controls allow the same performance (tracking). In transient mode, the backstepping command is better in terms of response time and overshoot.

Keywords Dual stator induction generator · Variable speed wind turbine · Maximum power point tracking · PI controller · Backstepping control

✉ Meryem Benakcha
benakcha.meryem@univ-msila.dz

[1] Electrical Engineering Laboratory LGE, M'sila University, BP 166, M'sila, Algeria

[2] Electrical Engineering Laboratory LGEB, Biskra University, BP 45, M'sila, Algeria

1 Introduction

In the last few decades, the intense industrialization and the multiplication of electric household appliances have led to considerable needs in terms of electrical energy. Faced with this demand, which is still growing today, the industrialized countries have relied heavily on nuclear power plants. This energy source has the undeniable advantage of not causing air pollution unlike thermal power plants, but the risk of nuclear accidents, the treatment of wastes are real problems which make this energy unattractive to the future generations (Ghoudelbourk et al. 2016). To face these problems, countries are increasingly turning to clean and renewable energy sources. Indeed, in the medium term, these countries undertook to increase the share of renewable energy in their electricity production (Miryousefi Aval et al. 2015; Mahboub et al. 2016). Among these renewable energy sources, wind energy is the one with the greatest energy potential (Tiwari and Babu 2016). The power of wind turbines installed in the world is increasing more and more every year. At present, horizontal axis wind turbines are much more used than vertical axis wind turbines for economic reasons related to their manufacture and installation (Hossain and Mohd 2015).

The studied system consists of horizontal axis wind turbine with variable speed connected to the grid through a DSIG. This type of multiphase machine, used in high power systems, and wind projects of which powers are of a few MW (Taheri 2016). It has several advantages compared with conventional alternative machines such as segmentation of the power, reducing the rotor harmonic currents and high reliability (Ameur et al. 2016; Lekhchine et al. 2014).

In term of wind energy and grid integration, it is very interesting to produce a quality output power. Therefore,

Published online: 18 July 2018

the control of the generator is very important. Many techniques have been used to control the DSIG such as a sliding mode control (SMC) associated to the field oriented control (Amimeur et al. 2012), Genetic Algorithm Optimized PI and Fuzzy Logic Speed Vector Control (Ameur and Kouzi 2013), model reference adaptive system based reactive power controller (Basak et al. 2014), nonlinear method based on the theory of fuzzy logic controlled torque (Chekkal et al. 2014), control of the DSIG using the instantaneous power theory and a control flux orientation at low speeds (Bu et al. 2015).

The objective of this work is the simulation of the entire wind conversion system using two different techniques to control the DSIG. The first technique uses a linear control based on the PI controller and the second technique is a relatively new nonlinear control based on backstepping controller used in mode generation. These techniques are used in order to compare the performances of the system in the two cases.

The mathematical model of the entire conversion system should be studied and detailed. The obtained results using Matlab/Simulink software will be examined and interpreted.

2 Description of the wind system

The variable speed wind system studied in this section is based on a DSIG machine as it is shown in Fig. 1. The turbine, via a gearbox, drives the DSIG, which is connected to the power grid directly by the stator through two static converters. These latest are connected to a grid side through a DC bus and a filter.

According to Fig. 1, two detailed controls are required to ensure the operation of the wind turbine.

3 Modeling of the wind turbine

The wind, with speed V, applied to the blades of the wind turbine, causes its rotation and creates a mechanical power on the shaft of the turbine, denoted P_t and expressed by (Elmansouri et al. 2015; Guediri and Ben Attous 2015):

$$P_t = 0.5C_p(\lambda)\rho SV^3 \tag{1}$$

Where the tip speed ratio λ is defined by:

$$\lambda = \frac{R\Omega_t}{V} \tag{2}$$

The power coefficient C_p represents the aerodynamic efficiency of the wind turbine and also depends on the characteristic of the turbine. This coefficient has a theoretical limit, called the *Betz* limit, equal to 0.593 and is never reached in practice (Kumar and Chatterjee 2016; Tria et al. 2017). We will use an approximate expression of the power coefficient as a function of the relative velocity λ' and of the blade angle β of which the following expression is (Tamaarat and Benakcha 2014):

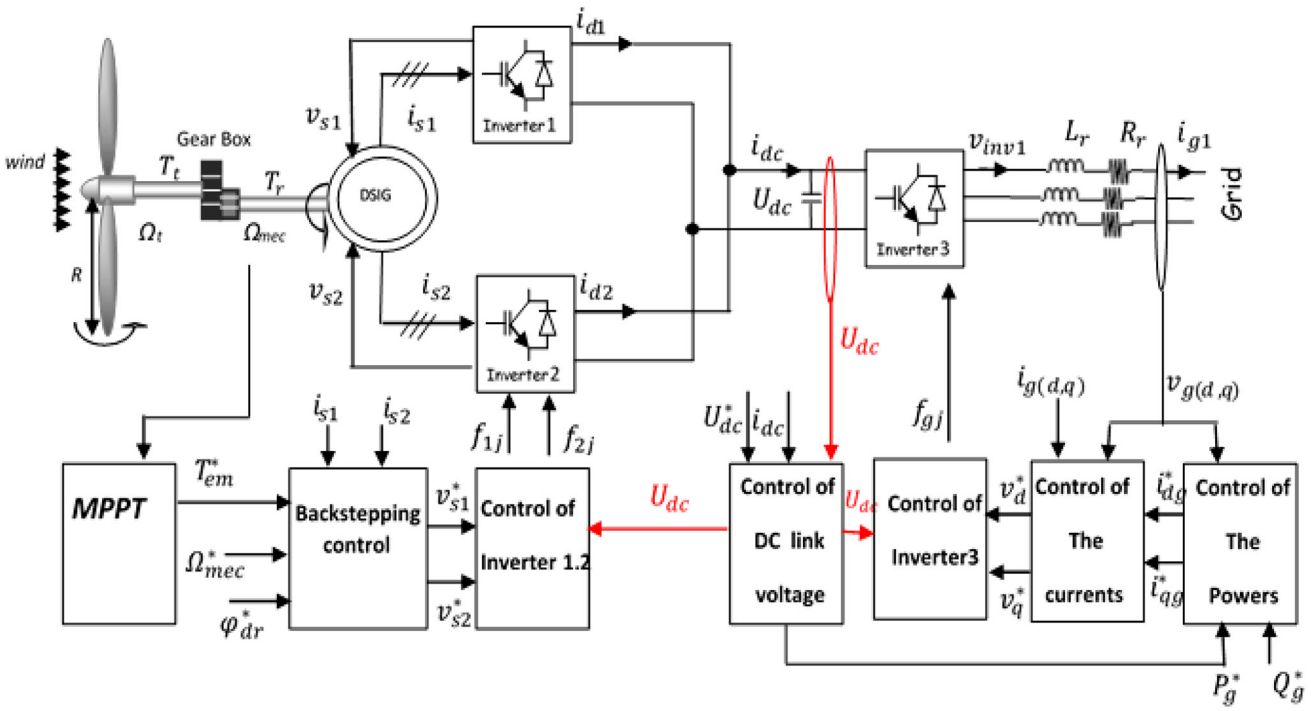

Fig. 1 Bloc diagram of the whole wind power conversion system based on DSIG

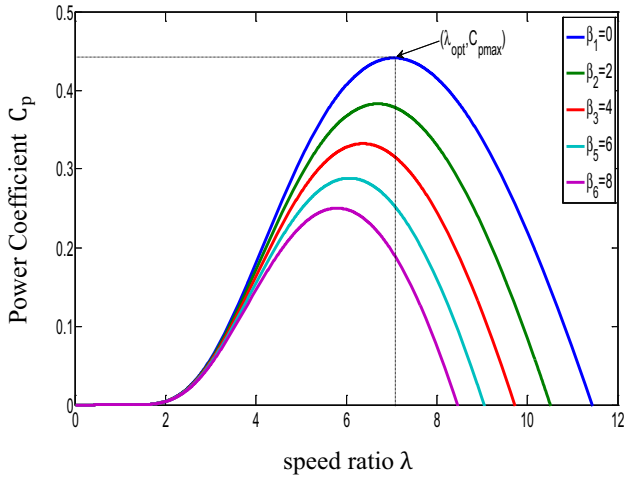

Fig. 2 The graph of C_p in function of λ

$$C_p = \left[0.73\left(\frac{151}{\lambda'}\right) - 0.002\beta - 13.2\right] exp\left(\frac{-18.4}{\lambda'}\right) \quad (3)$$

with

$$\lambda' = \left[1/(\lambda + 0.08\beta) - 0.035/(\beta^3 + 1)\right]^{-1}$$

For different values of the blade angle, the graph of the power coefficient in function of tip speed ratio $C_p(\lambda)$, given in Fig. 2, is plotted using expression (3).

The gearbox adapts the rotation speed of the turbine (slow shaft) to the rotation speed of the DSIG (fast shaft) (Fig. 3). Considering that the gearbox is ideal (the mechanical losses are negligible), we can model it by the two following expressions (Taraft et al. 2013):

$$T_g = \frac{T_t}{G},\ \Omega_t = \frac{\Omega_{\text{mec}}}{\text{G}} \quad (4)$$

For a given operating point, it is desired that the mechanical power be maximum.This corresponds to the maximum value of the power coefficient C_p. This is obtained if the relative velocity λ is equal to its optimal value λ_{opt} for $\beta = 0°$ (Errami et al. 2015).

4 Modeling of DSIG

The dual stator induction generator model is composed of two fixed three-phase stator windings displaced with an electrical angle $\alpha = 30°$ and a squirrel cage mobile rotor winding (Pandit et al. 2016; Ameur et al. 2016) as shown in (Fig. 4).

Considering the choice of the reference (dq) linked to the rotating field, a simplification of the DSIG expressions is obtained by writing a following compact form (Ameur and Kouzi 2013).

$$[\dot{I}] = [L]^{-1}\{[B][U] - \omega_{gl}[C][I] - [D][I]\} \quad (5)$$

where: $\omega_{gl} = \omega_s - \omega_r$, $\omega_r = p * \Omega_t$; $[U] = [v_{ds1}\, v_{qs1}\, v_{ds}\, 2v_{qs2}\, v_{dr}\, v_{qr}]^t$; $[I] = \left[i_{ds1}\, i_{qs1}\, i_{ds2}\, i_{qs2}\, i_{dr}\, i_{qr}\right]^t$; $[\dot{I}] = \frac{d}{dt}[I]$; $[B] = diag[111100]$,

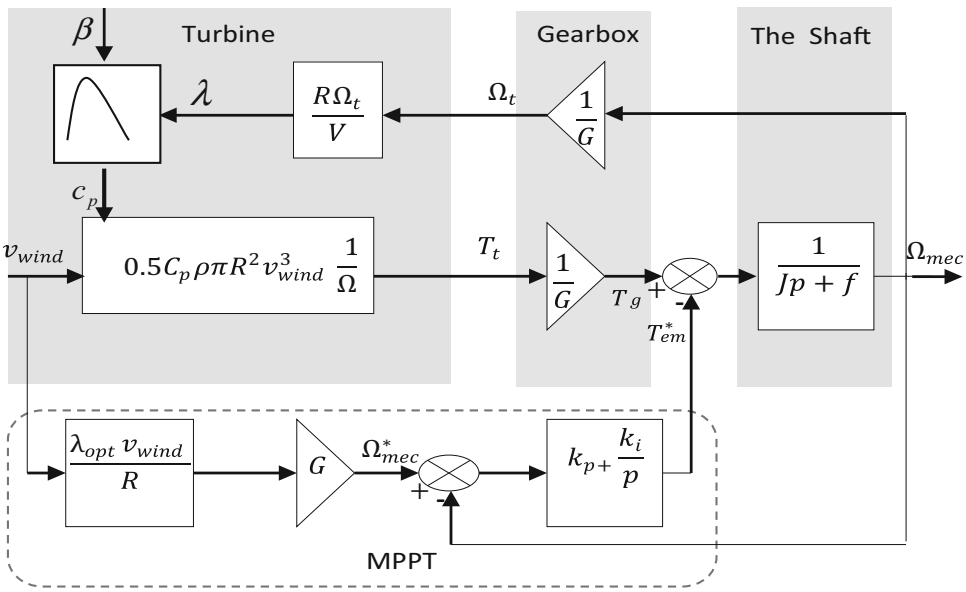

Fig. 3 Block diagram of the turbine model with variable speed control

$$[C] = \begin{bmatrix} 0 & 0 & 0 & 0 & 0 & 0 \\ 0 & 0 & 0 & 0 & 0 & 0 \\ 0 & 0 & 0 & 0 & 0 & 0 \\ 0 & 0 & 0 & 0 & 0 & 0 \\ 0 & -L_m & 0 & -L_m & 0 & -(L_r + L_m) \\ L_m & 0 & L_m & 0 & L_r + L_m & 0 \end{bmatrix}$$

$$[L] = \begin{bmatrix} (L_{s1} + L_m) & 0 & L_m & 0 & L_m & 0 \\ 0 & (L_{s1} + L_m) & 0 & L_m & 0 & L_m \\ L_m & 0 & (L_{s2} + L_m) & 0 & L_m & 0 \\ 0 & L_m & 0 & (L_{s2} + L_m) & 0 & L_m \\ L_m & 0 & L_m & 0 & (L_r + L_m) & 0 \\ 0 & L_m & 0 & L_m & 0 & (L_r + L_m) \end{bmatrix}$$

$$[D] = \begin{bmatrix} R_{s1} & -\omega_s(L_{s1} + L_m) & 0 & -\omega_s L_m & 0 & -\omega_s L_m \\ \omega_s(L_{s1} + L_m) & R_{s1} & \omega_s L_m & 0 & \omega_s L_m & 0 \\ 0 & -\omega_s L_m & R_{s2} & -\omega_s(L_{s2} + L_m) & 0 & -\omega_s L_m \\ \omega_s L_m & 0 & \omega_s(L_{s2} + L_m) & R_{s2} & \omega_s L_m & 0 \\ 0 & 0 & 0 & 0 & R_r & 0 \\ 0 & 0 & 0 & 0 & 0 & R_r \end{bmatrix}$$

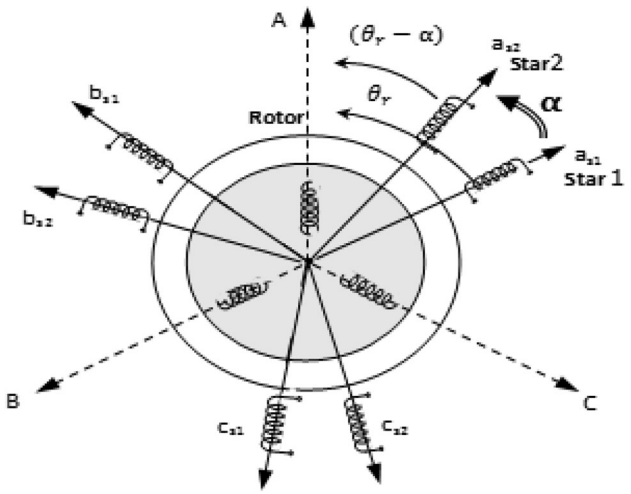

Fig. 4 Schematic model of dual stator induction generator

The electromagnetic torque is expressed as:

$$T_{em} = P\frac{L_m}{(L_m + L_r)}\left[(\imath_{qs1} + \imath_{qs2})\varphi_{dr} - (\imath_{ds1} + \imath_{ds2})\varphi_{qr}\right] \tag{6}$$

5 Field oriented control of DSIG

For the DSIG, we choose the orientation of the rotor flux, because this allows to obtain a variation of speed where the flux and the electromagnetic torque are independently controlled through the direct and quadratic stator currents, respectively (Mehammai et al. 2014; Bekakra and Ben Attous 2015).

Expressions of the electromagnetic torque and slip speed references are respectively (Amimeur et al. 2012):

$$T_{em}^* = P\frac{L_m}{(L_m + L_r)}\left(\imath_{qs1}^* + \imath_{qs2}^*\right)\varphi_r^*, \tag{7}$$

$$\omega_{sl}^* = \frac{r_r L_m}{L_m + L_r}\frac{(\imath_{qs1}^* + \imath_{qs2}^*)}{\varphi_r^*}, \tag{8}$$

With: $\imath_{ds1}^* + \imath_{ds2}^* = \frac{\varphi_r^*}{L_m}$,

We suppose that the two stars have the same values of the reference currents: $\imath_{ds1}^* = \imath_{ds2}^*, \imath_{qs1}^* = \imath_{qs2}^*$.

The references stator voltages are expressed by:

$$\begin{cases} v_{ds1}^* = PI(\imath_{ds1}^* - \imath_{ds1}) - \delta_1 \\ v_{qs1}^* = PI\left(\imath_{qs1}^* - \imath_{qs1}\right) + \delta_2 \\ v_{ds2}^* = PI(\imath_{ds2}^* - \imath_{ds2}) - \delta_3 \\ v_{qs2}^* = PI(\imath_{qs2}^* - \imath_{qs2}) + \delta_4 \end{cases} \tag{9}$$

where:

$$\begin{cases} \delta_1 = \omega_s^*\left(L_{s1}\imath_{qs1} + \tau_r\varphi_{dr}^*\omega_{sl}^*\right) \\ \delta_2 = \omega_s^*\left(L_{s1}\imath_{ds1} + \varphi_{dr}^*\right) \\ \delta_3 = \omega_s^*\left(L_{s2}\imath_{qs2} + \tau_r\varphi_{dr}^*\omega_{sl}^*\right) \\ \delta_4 = \omega_s^*\left(L_{s2}\imath_{ds2} + \varphi_{dr}^*\right) \end{cases}$$

6 Backstepping control of DSIG

The application of the Backstepping technique to the DSIG control consists in establishing a control law of the machine via a chosen Lyapunov function to guarantee the overall stability of the system (Herizi et al. 2015; Bouzidi et al. 2016).

A. Step1

In this step, we define the errors e_1 and e_2 representing the error between the reference speed and the actual speed and the error between reference direct rotor flux and its actual value respectively.

$$\begin{cases} e_1 = \Omega^* - \Omega_{mec} \\ e_2 = \varphi_{dr}^* - \varphi_{dr} \end{cases} \tag{10}$$

The first Lyapunov function is chosen as:

$$V_1 = \frac{1}{2}(e_1^2 + e_2^2) \tag{11}$$

Its derivative is:

$$\begin{aligned} \dot{V}_1 &= e_1\dot{e}_1 + e_2\dot{e}_2 \\ &= e_1[\dot{\Omega}^* - \frac{1}{J}\left[\mu\left(\imath_{qs1} + \imath_{qs2}\right)\varphi_{dr}^* - T_r - f_r\Omega\right] \\ &\quad + \left[\dot{\varphi}_{dr}^* - [-\gamma\varphi_{dr} + \gamma L_m(\imath_{ds1} + \imath_{ds2})]\right] \end{aligned} \tag{12}$$

The tracking objectives $\dot{V}_1 < 0$ are achieved by choosing the references of the current components that represent the stabilizing functions, as follows:

$$\begin{cases} \imath_{qs1}^* + \imath_{qs2}^* = \dfrac{J}{\mu\varphi_{dr}^*}\left[K_1 e_1 + \dot{\Omega}^* + \dfrac{T_r}{J} + \dfrac{f_r\Omega}{J}\right] \\ \imath_{ds1}^* + \imath_{ds2}^* = \dfrac{1}{\gamma L_m}\left[K_2 e_2 + \dot{\varphi}_{dr}^* + \gamma\varphi_{dr}\right] \end{cases} \tag{13}$$

where: K_1, K_2 are positive constants; $\mu = \frac{L_m}{L_m + L_r}$, $\gamma = \frac{r_r}{L_r + L_m}$

B. Step2:

For this step, we eliminate the PI current regulators (similar as in Fig. 5) by calculating the control voltages. Other errors concerning the components of the stator current and their references are defined as:

$$\begin{cases} e_3 = \imath_{qs1}^* - \imath_{qs1} \\ e_4 = \imath_{ds1}^* - \imath_{ds1} \\ e_5 = \imath_{qs2}^* - \imath_{qs2} \\ e_6 = \imath_{ds2}^* - \imath_{ds2} \end{cases} \tag{14}$$

The final Lyapunov function is given by:

$$V_2 = \frac{1}{2}(e_1^2 + e_2^2 + e_3^2 + e_4^2 + e_5^2 + e_6^2) \tag{15}$$

Its derivative in function of time is:

$$\begin{aligned} \dot{V}_2 &= e_1\dot{e}_1 + e_2\dot{e}_2 + e_3\dot{e}_3 + e_4\dot{e}_4 + e_5\dot{e}_5 + e_6\dot{e}_6 \\ \dot{V}_2 &= -K_1e_1^2 - K_2e_2^2 - K_3e_3^2 - K_4e_4^2 - K_5e_5^2 - K_6e_6^2 \\ &\quad + e_3\left(K_3e_3 - \sigma_1 + \dot{i}_{qs1}^* - \frac{1}{L}v_{qs1}\right) \\ &\quad + e_4\left(K_4e_4 - \sigma_2 + \dot{i}_{ds1}^* - \frac{1}{L}v_{ds1}\right) \\ &\quad + e_5\left(K_5e_5 - \sigma_3 + \dot{i}_{qs2}^* - \frac{1}{L}v_{qs2}\right) \\ &\quad + e_6\left(K_6e_6 - \sigma_4 + \dot{i}_{ds2}^* - \frac{1}{L}v_{ds2}\right) \end{aligned} \tag{16}$$

where:

$$\begin{cases} \sigma_1 = \dfrac{1}{L_1}\left\{-r_1\imath_{qs1} - \omega_s^*\left(L_1\imath_{ds1} + \varphi_{dr}^*\right)\right\} \\ \sigma_2 = \dfrac{1}{L_1}\left\{-r_1\imath_{ds1} + \omega_s^*\left(L_1\imath_{qs1} + \tau_r\varphi_{dr}^*\omega_{sl}^*\right)\right\} \\ \sigma_3 = \dfrac{1}{L_2}\left\{-r_2\imath_{qs2} - \omega_s^*\left(L_2\imath_{ds2} + \varphi_{dr}^*\right)\right\} \\ \sigma_4 = \dfrac{1}{L_2}\left\{-r_2\imath_{ds2} + \omega_s^*\left(L_2\imath_{qs2} + \tau_r\varphi_{dr}^*\omega_{sl}^*\right)\right\} \end{cases}$$

The control voltages are selected as follows:

$$\begin{cases} v_{qs1}^* = L_1\left[K_3e_3 - \sigma_1 + \dot{i}_{qs1}^*\right] \\ v_{ds1}^* = L_1\left[K_4e_4 - \sigma_2 + \dot{i}_{ds1}^*\right] \\ v_{qs2}^* = L_2\left[K_5e_5 - \sigma_3 + \dot{i}_{qs2}^*\right] \\ v_{ds2}^* = L_2\left[K_6e_6 - \sigma_4 + \dot{i}_{ds2}^*\right] \end{cases} \tag{17}$$

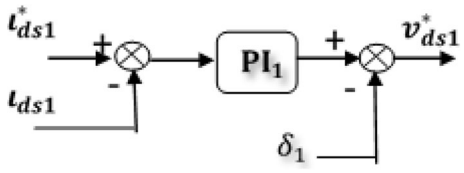

Fig. 5 Design of the current $\imath_{ds1}$ using *PI* controller

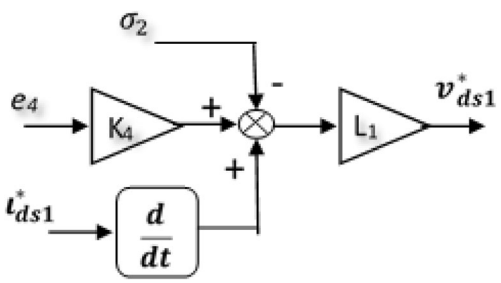

Fig. 6 Design of the current $\imath_{ds1}$ using the backstepping controller

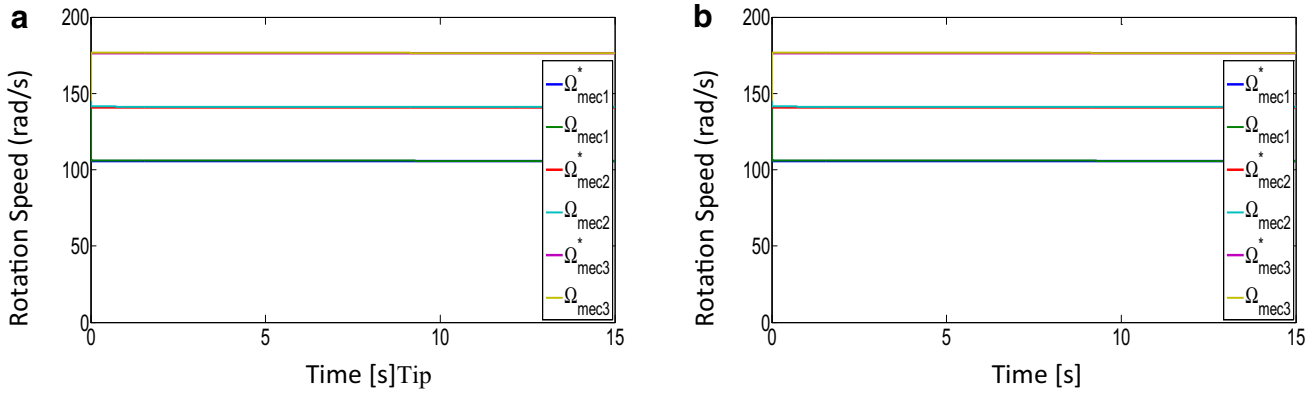

Fig. 7 DSIG speed and its reference for three constant speeds

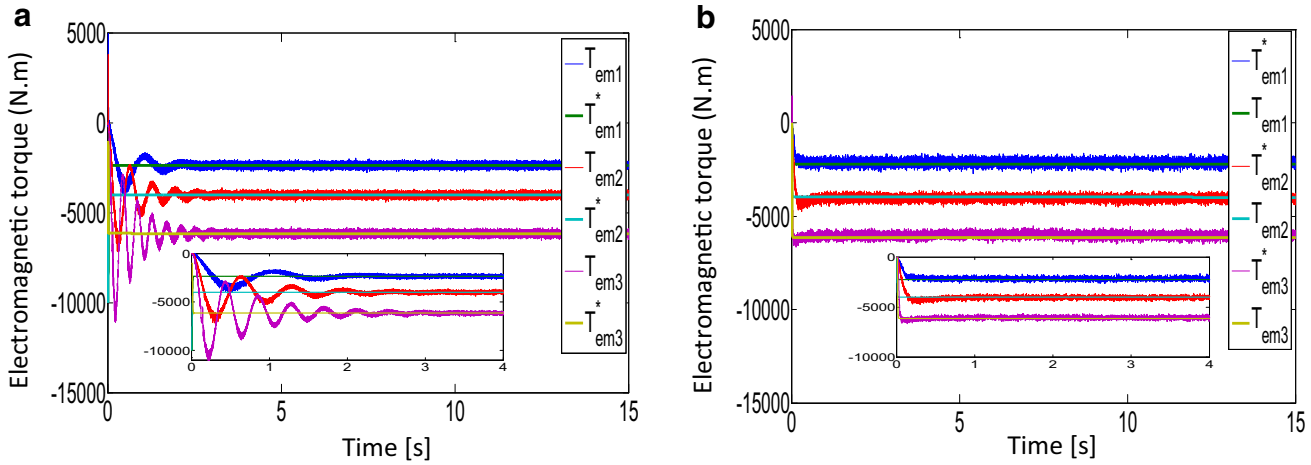

Fig. 8 DSIG Torque and its reference for three constant speeds

The stability of the control is obtained if and only if a good choice of the gains K_3, K_4, K_5, K_6 is made. Figure 6 represents the current regulator configuration.

7 Grid side control

The objective of the DC bus control loop is to set the voltage constant. This voltage becomes a power source of the DSIG to ensure the correct operation of the converters and to impose an operation with an active reference power equal to that generated by the system of wind energy conversion.

The value of the DC bus voltage is obtained from the integration of the capacitive current (Kammoun et al. 2017).

$$U_{dc} = \frac{1}{C}\int \imath_c dt \tag{18}$$

where:

$$\imath_c = \imath_{dc} - \imath_{inv}$$

The grid reference active power is:

$$P^*_g = U_{dc}\imath_{dc} - U_{dc}\imath^*_{dc} \tag{19}$$

where the tuning of the DC link is carried out by a regulation loop, using a PI corrector, which generates the capacitive current reference ($\imath^*_{dc}$) in the capacitor:

$$\imath^*_{dc} = PI(s)(U^*_{dc} - U_{dc}) \tag{20}$$

Network reference currents expressions can be represented by:

$$\begin{cases} \imath^*_{dg} = \dfrac{P^*_g v_{dg} + Q^*_g v_{qg}}{v^2_{dg} + v^2_{qg}} \\ \imath^*_{qg} = \dfrac{P^*_g v_{qg} - Q^*_g v_{dg}}{v^2_{dg} + v^2_{qg}} \end{cases}, \tag{21}$$

The reference voltages expressed in d-q frame reference are given by:

$$\begin{cases} v^*_{d\_inv} = v^*_{dg} + v_{dg} - \omega_s L_f \imath_{qg} \\ v^*_{q\_inv} = v^*_{qg} + v_{qg} + \omega_s L_f \imath_{dg} \end{cases} \tag{22}$$

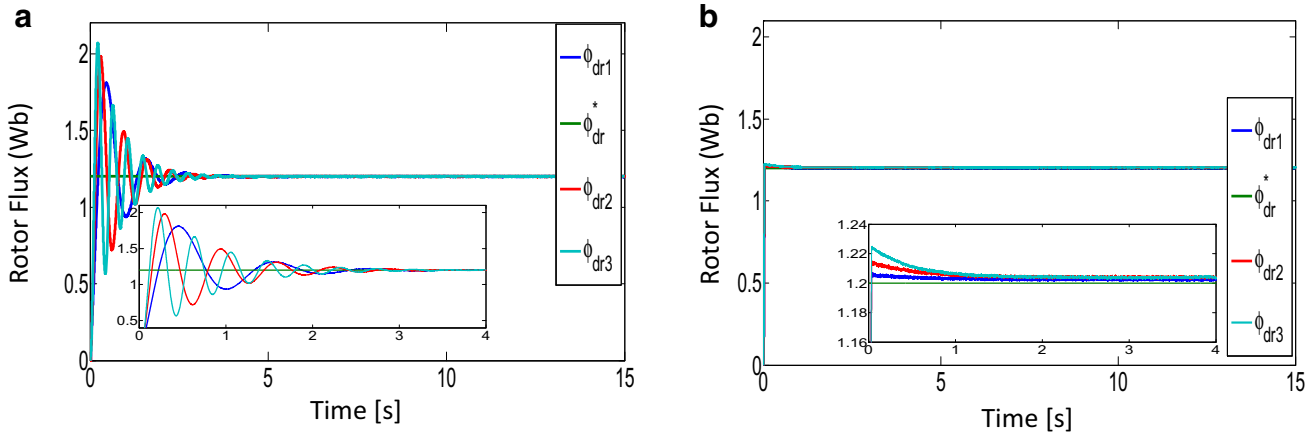

Fig. 9 Direct rotor flux and its reference for three constant speeds

Table 1 Summarization table of the response time and overshoot of the two control strategies applied to the DSIG

	V1 = 6 m/s		V2 = 8 m/s		V3 = 10 m/s	
	Tr(s)	D	Tr(s)	D	Tr(s)	D
PI control						
Tem (Nm)	0.2425	1085	0.1652	2470	0.1444	4219
Flux (Wb)	0.2119	0.6080	0.1418	0.781	0.1146	0.866
Backstepping control						
Tem (Nm)	0.1533	0.0000	0.1395	0.000	0.0488	0.000
Flux (Wb)	0.0322	0.0050	0.0321	0.014	0.0320	0.024

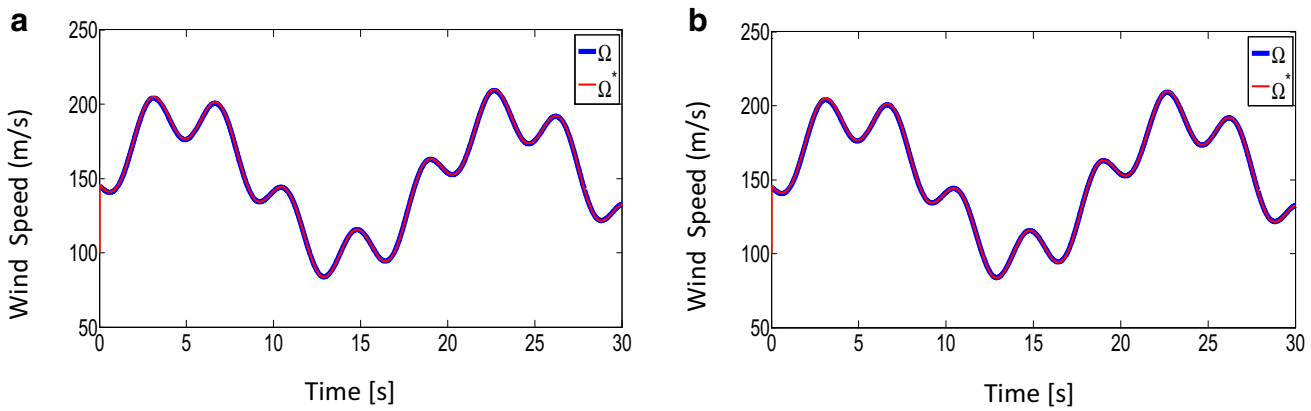

Fig. 10 DSIG speed and its reference

where:

$$\begin{cases} v^{*}_{dg} = PI(s)(\imath^{*}_{dg} - \imath_{dg}) \\ v^{*}_{qg} = PI(s)(\imath^{*}_{qg} - \imath_{qg}) \end{cases}$$

8 Simulation results and discussion

The proposed control algorithm has been simulated using Matlab/Simulink software. The DSIG used in this work, rated at 1.5 MW and whose nominal parameters are indicated in appendix, is simulated choosing $\alpha = 30°$.

The simulation results show a comparative study of the classical PI control and the backstepping control strategies of the dual stator induction generator integrated in wind energy conversion system.

The Figures are specified (a) for PI control and (b) for backstepping control. To compare the performances of them, the first test of the entire system uses three fixed wind speeds (6, 8, and 10 m/s). Figure 7 presents the rotation speed of DSIG for different wind speeds and their references. It can be seen from (Figs. 8 and 9) that the backstepping control responds faster than PI control at low,

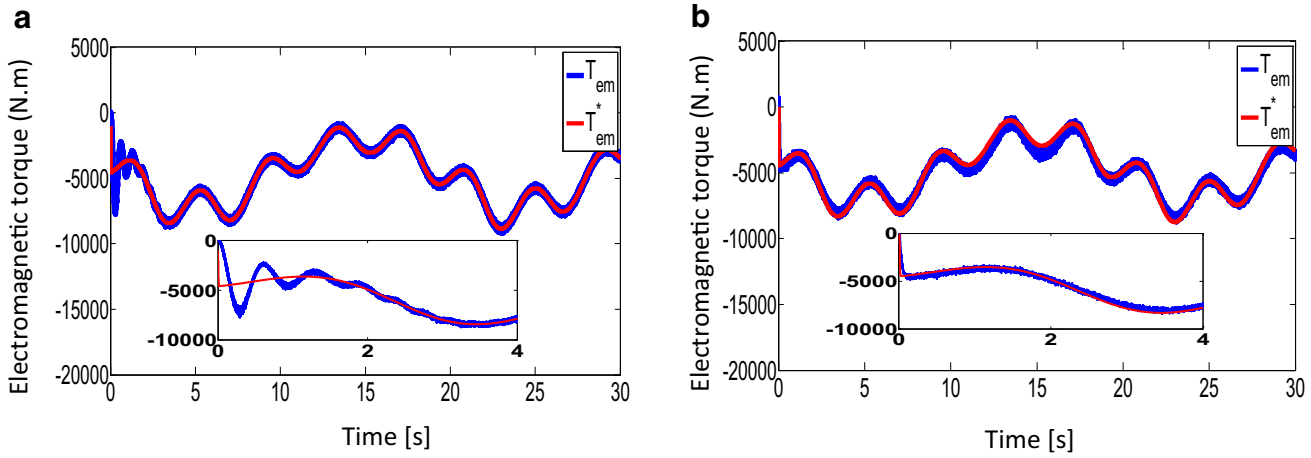

Fig. 11 DSIG torque and its reference

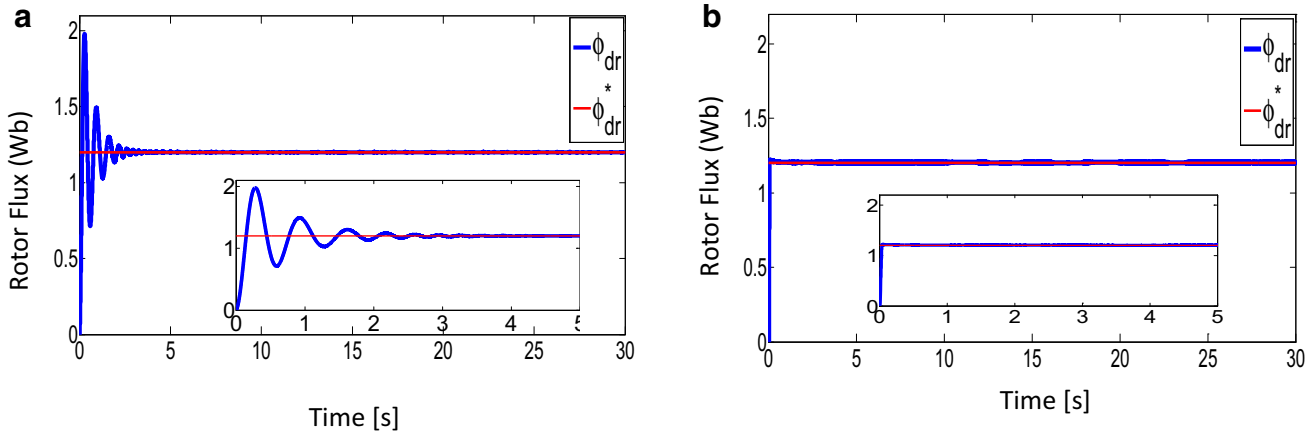

Fig. 12 Direct and quadratic rotor flux

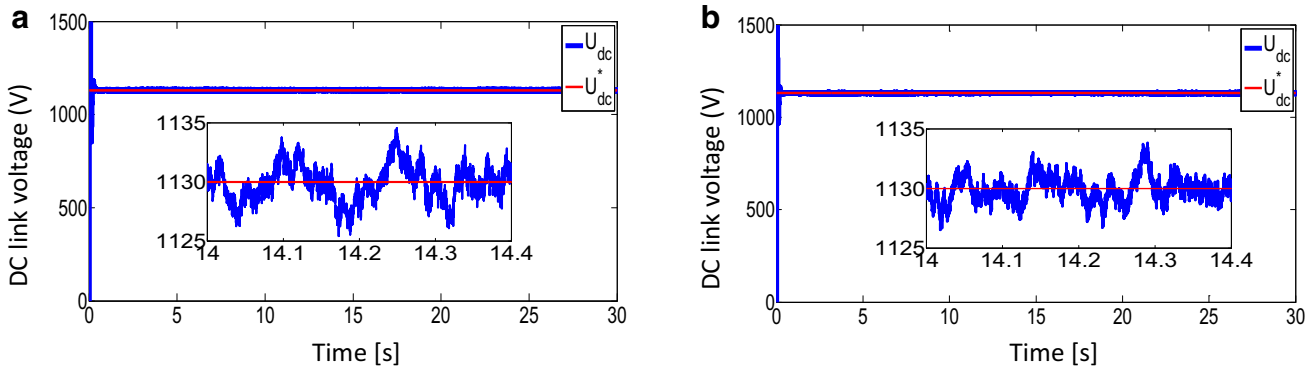

Fig. 13 DC link voltage

medium and high wind speeds and for both controls, the response time (Tr) is improved when the wind speed increases. It indicates also that the backstepping control eliminates the overshoot (D). It does not require any torque limiter. This is obviously not the case of the PI control where the overshoot increases with the wind speed, meaning that the DSIG delivers faster with the backstepping control than with the PI control and delivers faster when the wind speed increases. The synthesis of this analysis is summarized in the Table 1.

The second test (Fig. 10) is conducted using the wind variable speed profile. The figures are specified (a) for the

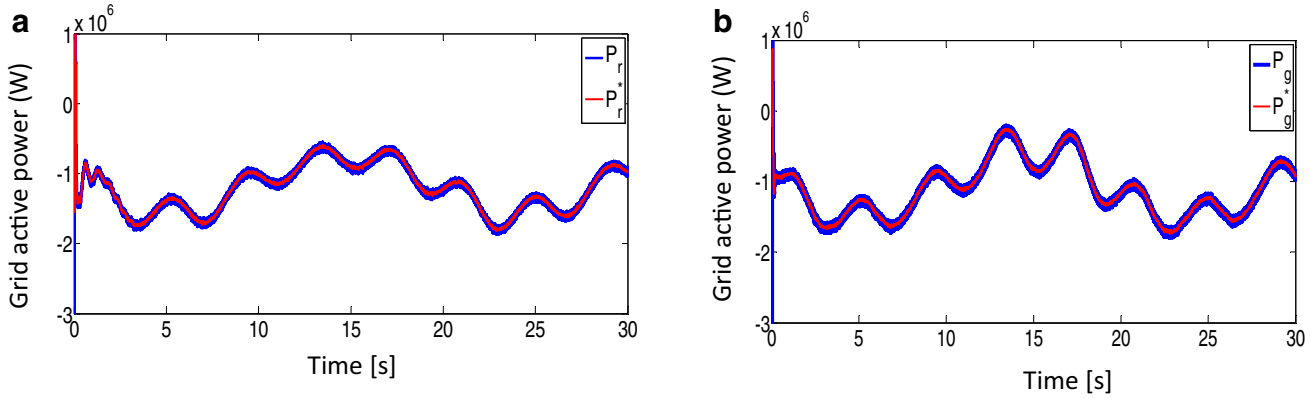

Fig. 14 Grid active power

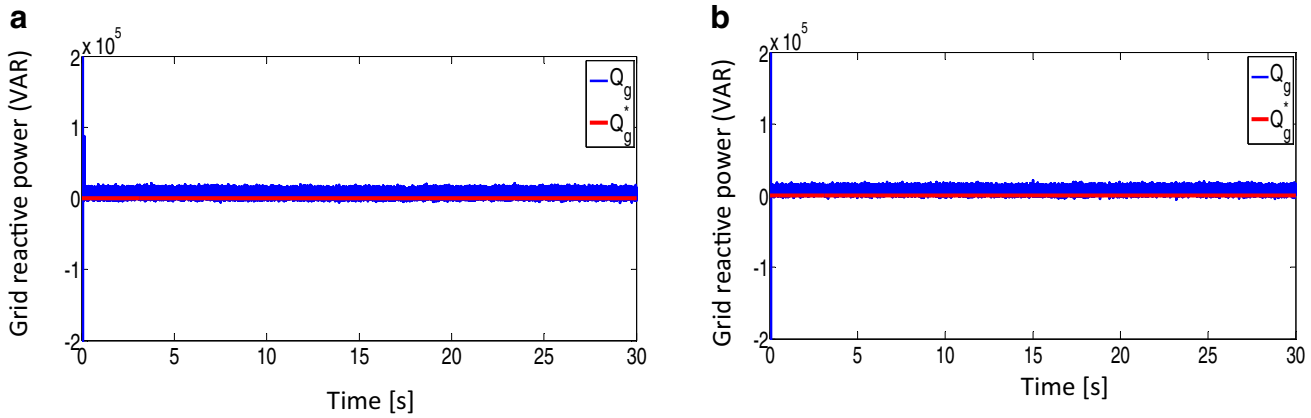

Fig. 15 Grid reactive power

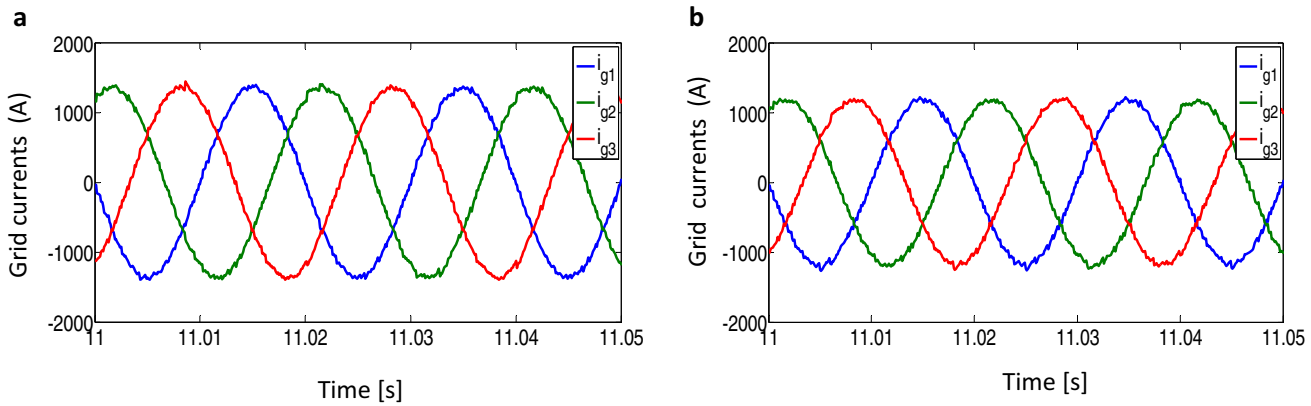

Fig. 16 Currents in the three phase's grid

PI control and (b) for the backstepping control. It is clear from this figure that the rotation speed follows perfectly its reference, which varies depending on the imposed wind profile. The waveform of the electromagnetic torque generator follows its reference resulting from the MPPT algorithm, as shown in (Fig. 11). The direct rotor flux and its reference of the DSIG are illustrated in (Fig. 12). The DC link voltage is constant and follows its set level 1130 V (Fig. 13). It can be seen from (Figs. 14 and 15) that the active and reactive grid powers, respectively, follow in an acceptable way in accordance to their references at all simulation time. In order to get a unit power-factor in

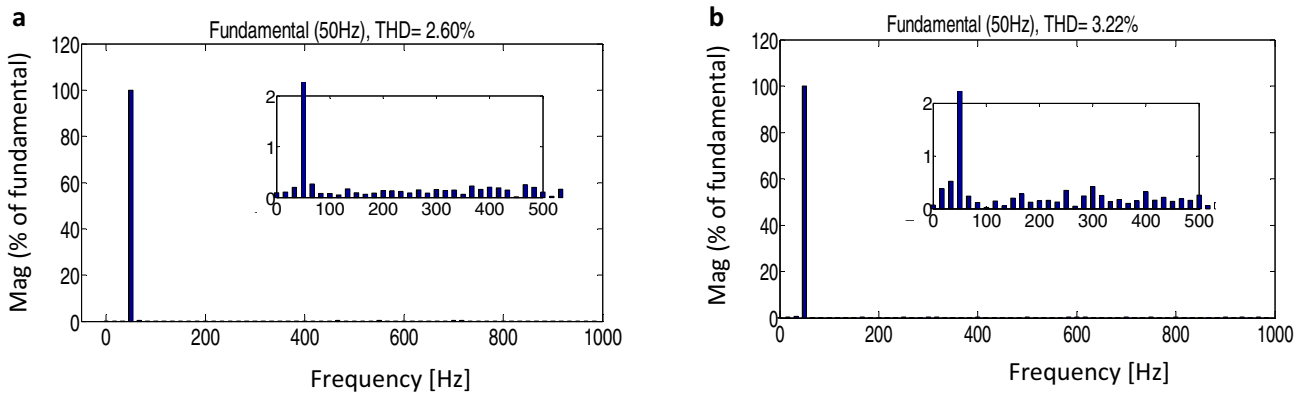

Fig. 17 THD of the grid current

network side, the reactive power reference Q_g^* is fixed at zero value. For the proposed algorithms the currents in the three phase's grid, illustrated in Fig. 16, constitute a sinusoidal and a balanced system of the frequency 50 Hz.

Figure 17 in turn, gives the THD (total harmonic distortion) of the grid current Ig1. This THD is defined as the ratio of total effective value of harmonics (their quadratic sum) to the rms value of the fundamental component. We analyze a sequence of time. As we see, the harmonics appearing in the grid current are minimized. We notice also that the THD of PI control is lower than the THD of Backstepping control.

9 Conclusion

This paper discusses synthesis of linear (based on the PI control) and nonlinear control (based on backstepping control) of a DSIG dedicated to a wind turbine system. The two control laws are applied to the stator side inverters. We define the complete model of the wind system by integrating the previous process, adjusting the DC link voltage and controlling the active and reactive powers to the grid side converter. All system is delivering into the grid. Finally, the results for the two approaches have been discussed and compared. The responses of the system show a significant overshoot for the electromagnetic torque and the rotor flux at the starting up for the PI control, while for the backstepping control, the trajectory tracking is done without any overshoot.

The observation of the different results obtained shows a good behavior of the system for the PI control. However, the backstepping strategy has better dynamic performances.

Appendix: Parameters

Radius of the turbine	R = 36 m
Gear box gain	G = 90
Maximum power coefficient	$C_{pmax} = 0.44$
Optimal relative wind speed	$\lambda_{opt} = 7.05$
DSIG nominal power	$P_n = 1.5$ MW
RMS voltage value	U = 400 V
Frequency	F = 50 Hz
Number of pole pairs	p = 2
Stator resistance	$R_{s1} = R_{s2} = 0.008\ \Omega$
Stator inductance	$L_{s1} = L_{s2} = 0.134$ mH
Magnetizing inductance	$L_m = 0.0045$ H
Rotor resistance	$R_r = 0.007\ \Omega$
Rotor inductance	$L_r = 0.067$ mH
Inertia	J = 10 kg.m^2
Viscous coefficient	f = 2.5 Nm s/rd
Filter inductance	$L_f = 0.001$ H
Filter resistance	$R_f = 0.01\ \Omega$
Capacitance of the DC link voltage	C = 0.072 F

References

Ameur F, Kouzi K (2013) Genetic algorithm optimized PI and fuzzy logic speed vector control of dual stator induction generator in wind energy conversion system. In: Proceedings of the 3rd international conference on systems. Algiers, October 29–31

Ameur F, Kouzi K, Ameur A, Kasbadji NM (2016) Robust control of dual stator induction generator used in wind conversion system connectes to the grid usin direct torque control. In: 4th International conference on renewable energy: generation and applications ICREGA'16, At Belfort, Franch

Amimeur H, Aouzellag D, Abdessemed R, Ghedamsi K (2012) Sliding mode control of a dual-stator induction for wind energy conversion systems. Electr Power Energy Syst 42:60–70

Basak S, Chakraborty C, Sinha AK (2014) Dual stator induction generator with controllable reactive power capability. In: 23rd International symposium on industrial electronics (ISIE), IEEE

Bekakra Y, Ben Attous D (2015) Optimizing of IP speed controller using particle swarm optimization for FOC of an induction motor. Int J Syst Assur Eng Manag. https://doi.org/10.1007/s13198-015-0391-1

Bouzidi M, Benaissa A, Barkat S, Bouafia S, Bouzidi A (2016) Virtual flux direct power control of the three-level NPC shunt active power filter based on backstepping control. Int J Syst Assur Eng Manag. https://doi.org/10.1007/s13198-016-0433-3

Bu F, Hu Y, Huang W, Zhuang S, Shi K (2015) Wide-speed-range-operation dual stator-winding induction generator DC generating system for wind power applications. IEEE Trans Power Electron 30(2):561–573

Chekkal S, Aouzellag Lahaçani N, Aouzellag D, Ghedamsi K (2014) Fuzzy logic control strategy of wind generator based on the dual stator induction generator. Electr Power Energy Syst 59:166–175

Elmansouri A, El mhamdi J, Boualouch A (2015) Control by back stepping of the DFIG used in the wind turbine. Int J Emerg Technol Adv Eng 5(2):472–478

Errami Y, Ouassaid M, Maaroufi M (2015) Optimal power control strategy of maximizing wind energy tracking and different operating conditions for permanent magnet synchronous generator wind farm. Energy Procedia 74:477–490

Ghoudelbourk S, Dib D, Omeiri A, Azar AT (2016) MPPT control in wind energy conversion systems and the application of fractional control (PI^{α}) in pitch wind turbine. IntJ Model Identif Control 26(2):140–151

Guediri AK, Ben Attous D (2015) Modeling and fuzzy control of a wind energy system based on double- fed asynchronous machine for supply of power to the electrical network. Int J Syst Assur Eng Manag. https://doi.org/10.1007/s13198-015-0367-1

Herizi A, Balla R, Ahmani SA (2015) Backstepping control of induction motors. El Wahat pour les Recherches et les Etudes 8:132–145

Hossain MM, Mohd HA (2015) Future research directions for the wind turbine generator system. Renew Sustain Energy Rev 49:481–489

Kammoun S, Sallem S, Kammoun MBK (2017) Backstepping control for low-voltage ride through enhancement of DFIG-based wind turbines. Arab J Sci Eng. https://doi.org/10.1007/s13369-017-2606-z

Kumar D, Chatterjee K (2016) A review of conventional and advanced MPPT algorithms for wind energy systems. Renew Sustain Energy Rev 55:957–970

Lekhchine S, Bahi T, Soufi Y (2014) Indirect rotor field oriented control based on fuzzy logic controlled double star induction machine. Electr Power Energy Syst 57:206–211

Mahboub MA, Drid S, Sid MA, Cheikh R (2016) Sliding mode control of grid connected brushless doubly fed induction generator driven by wind turbine in variable speed. Int J Syst Assur Eng Manag. https://doi.org/10.1007/s13198-016-0524-1

Mehammai C, Zidani F, Benaicha S, Nait-Said MS (2014) Research on improvement of FOC system for induction motor using fuzzy logic. Int J Modell Identif Control 21(4):370–377

Miryousefi Aval SM, Ahadi A, Hayati H (2015) A novel method for reliability and risk evaluation of wind energy conversion systems considering wind speed correlation. Front Energy. https://doi.org/10.1007/s11708-015-0384-4

Pandit JK, Aware MV, Levi RE (2016) Direct torque control scheme for a six-phase induction motor with reduced torque ripple. IEEE Trans Power Electron. https://doi.org/10.1109/TPEL.2016.2624149

Taheri A (2016) Harmonic reduction of direct torque control of six-phase induction motor. ISA Trans. https://doi.org/10.1016/j.isatra.2016.02.014i

Tamaarat A, Benakcha A (2014) Performance of PI controller for control of active and reactive power in DFIG operating in a grid-connected variable speed wind energy conversion system. Front Energy 8(3):371–378

Taraft S, Rekioua D, Aouzellag D (2013) Wind power control system associated to the flywheel energy storage system connected to the grid. Energy Procedia 36:1147–1157

Tiwari R, Babu NR (2016) Recent developments of control strategies for wind energy conversion system. Renew Sustain Energy Rev 66:268–285

Tria FZ, Srairi K, Benchouia MT, Benbouzid MEH (2017) An integral sliding mode controller with super-twisting algorithm for direct power control of wind generator based on a doubly fed induction generator. DOI, Int J Syst Assur Eng Manag. https://doi.org/10.1007/s13198-017-0597-5